J Biol Inorg Chem (2015) 20:555–562
DOI 10.1007/s00775-015-1240-z

ORIGINAL PAPER

Theoretical insights into the mechanism of redox switch in heat shock protein Hsp33

Mironel Enescu · Rima Kassim · Christophe Ramseyer · Bruno Cardey

Received: 29 October 2014 / Accepted: 10 January 2015 / Published online: 31 January 2015

Abstract Heat shock protein 33 (Hsp33) is activated in the presence of H_2O_2 by a very interesting redox switch based on a tetra-coordinated zinc–cysteine complex present in the fully reduced and inactive protein form. The oxidation of this zinc center by H_2O_2 induces formation of two S–S bridges and the zinc release followed by the protein unfolding. We report here a theoretical study of the step-by-step sequence of the overall process starting with the oxidation of the first cysteine residue and ending with the zinc release. Each reaction step is characterized by its Gibbs free energy barrier ($\Delta G^{\ddagger}$). It is predicted that the first reaction step consists in the oxidation of Cys263 by H_2O_2 which is by far the most reactive cysteine ($\Delta G^{\ddagger} = 15.4$ kcal mol^{-1}). The next two reaction steps are the formation of the first S–S bridge between Cys263 and Cys266 ($\Delta G^{\ddagger} = 13.6$ kcal mol^{-1}) and the oxidation of Cys231 by H_2O_2 ($\Delta G^{\ddagger} = 20.4$ kcal mol^{-1}). It is then shown that the formation of the second S–S bridge (Cys231–Cys233) before the zinc release is most unlikely ($\Delta G^{\ddagger} = 34.8$ kcal mol^{-1}). Instead, the release of zinc just after the oxidation of the third cysteine (Cys231) is shown to be thermodynamically (dissociation Gibbs free energy $\Delta G_d = 6.0$ kcal mol^{-1}) and kinetically (reaction rate constant $k_d \approx 10^6$ s^{-1}) favored. This result is in good agreement with the experimental data on the oxidation mechanism of Hsp33 zinc center available to date.

Keywords Hsp33 · Redox switch · Hydrogen peroxide · Ab initio · Energy barrier

Introduction

Redox switches are molecular tools involved in the regulation of many proteins such as transcriptional regulators, chaperones or metabolic enzymes [1–3]. They belong to the cell defense system against the oxidative stress related to the high cellular levels of reactive oxygen species (ROS). Very often, the redox switches are based on the oxidation of thiol groups carried by the cysteine residues. This oxidation induces significant changes in the protein conformation and thus in its activity. The participation of thiols as main functional elements in many redox switches can be explained by two specific properties of these groups: (a) their reactivity is strongly dependent on their protonation state [4] that is efficiently controlled by the protein environment [5] and (b) the oxidized thiols can form S–S covalent bonds (S–S bridges) that are generally associated with important protein conformational changes [6].

The oxidative activation of the heat shock protein 33 (Hsp33) is a spectacular illustration of the redox switch principle. Hsp33 is a cytosolic chaperone present in a large

Electronic supplementary material The online version of this article (doi:10.1007/s00775-015-1240-z) contains supplementary material, which is available to authorized users.

M. Enescu (✉) · C. Ramseyer · B. Cardey
Laboratoire Chrono Environnement UMR CNRS 6249, University of Franche-Comté, 16 route de Gray, 25030 Besançon Cedex, France
e-mail: mironel.enescu@univ-fcomte.fr

C. Ramseyer
e-mail: christophe.ramseyer@univ-fcomte.fr

B. Cardey
e-mail: bruno.cardey@univ-fcomte.fr

R. Kassim
Centre de Recherche Universitaire de Djibouti (CRUD), University of Djibouti, Avenue Georges Clemenceau, Djibouti, Djibouti
e-mail: rima_kassim@univ.edu.dj

number of bacteria and that protects proteins against the oxidative aggregation induced by reactive chlorine species or by a combination of hydrogen peroxide (H_2O_2) and elevated temperatures [7, 8]. The reduced form of the protein is monomeric and presents a highly compact C-terminal domain that conceals the substrate-binding site thus rendering the protein chaperone inactive [9]. The structure of the reduced Hsp33 is stabilized by a zinc center containing four cysteine residues in their highly reactive state where the thiol group is unprotonated (thiolate form) [10]. The main stages in the Hsp33 activation mechanism have already been identified [9, 11–13]: the oxidation of thiolate groups by H_2O_2 or other oxidizing agents leads to the formation of two S–S bridges accompanied by the release of zinc. In the absence of the stabilizing zinc center, the protein unfolds and exposes its binding sites. The monomeric oxidized form has only partial chaperone activity. The protein activation is complete in its dimer form (formed before the binding to the substrate) that is the stable form of the oxidized Hsp33. However, several interesting questions about the details of this mechanism still remain in regard [1]. Are all the zinc coordinated cysteines equally redox sensitive? If the S–S bridges formation and the zinc release occur simultaneously [10], how do we explain the fact that the S–S bridges always connect the next neighbor cysteines (Cys231–Cys233 and Cys263–Cys266, residues notation as in Ref. [10])? The latter question is logical since in this case the S–S bonds will be formed inside the zinc cluster when the distances between the different cysteine residues are equivalent. Finally, what is the exact sequence of oxidation reactions here involved?

Waiting for further challenging experimental studies, we propose here a theoretical approach that is expected to provide a preliminary clarification of the problem. Obviously, performing quantum chemistry calculations of such a complex system with chemical precision is also a challenge. We have recently shown [14] that the energy barriers for the oxidation of zinc–thiolate complexes can be calculated with high precision based on the density functional theory (DFT) method and using the mPW1PW91 functional [15]. The effects of the protein environment can be further included by means of hybrid calculations combining the DFT and a molecular mechanics [16, 17] or a semi-empirical method [18–20]. Such a hybrid calculation mixing the DFT method (based on the mPW1PW91 functional) and the semi-empirical method PM6 [21] was successfully used for modeling the oxidation of the zinc–cysteine cluster in the β-domain of metallothionein [22]. Here, we use the same method to calculate the energy barriers for the oxidation by H_2O_2 of the four cysteines in the zinc complex of Hsp33. The problem of S–S bridges formation inside this complex is also considered and a sequence of probable reaction steps leading to the zinc release is finally proposed.

Computational method

The X-ray diffraction structure of Hsp33 used as reference in the present work is that reported by Jaroszewski et al. [10]. It contains 290 amino acid residues. The simplified system chosen in our calculations for representing the redox sensitive center includes the zinc atom and all protein residues within a sphere of 17 Å around the metal. The residues belonging to this selection form two strands: one containing 7 residues, Lys228-Tyr229-Lys230-Cys231-Asp232-Cys233-Asn234-Arg235 and another one which contains 11 residues, Val261-Val262-Cys263-Lys264-Trp265-Cys266-Asn267-Thr268-Arg269-Tyr270-Val271. The terminal residues in the two strands were capped with $–CH_3$ groups. Obviously, in the absence of its natural environment, this protein fragment can adopt a denatured conformation. Hence, during the geometry optimization of this system it is necessary to add constraints to preserve a realistic conformation, while preserving a satisfactory flexibility. In the case of cysteine oxidation by H_2O_2, the interaction between the two reactants is expected to induce only minor displacements, if any, of the protein backbone. Consequently, the N atoms belonging to the protein backbone were frozen during the geometry optimizations related to this reaction. On the other hand, the formation of S–S bridges requires much more protein flexibility. In this case, the geometry optimizations were performed by frizzing only the four terminal atoms (C or N) of the two strands.

All calculations were performed with the Gaussian 09 program [23] using the hybrid method integrated molecular orbital and molecular orbital (IMOMO) [24], version ONIOM [25]. In our case, the reaction core (the model system) is treated at the mPW1PW91/6-311 + $G(d, p)$ level of theory while the real system (the whole protein fragment) is treated at the semi-empirical level of theory PM6. The reaction core of the protein initially contains the thiolate groups $–CH_2S^-$ carried by the four cysteine residues and the zinc cation Zn^{2+} (Fig. 1). The starting configuration of the whole system was extracted from the reference structure. All optimizations were performed in vacuo, then the energy in aqueous solution was obtained by single point energy calculations using the polarisable continuum model (PCM) of Cossi et al. [26]. The Gibbs free energy in aqueous solution of the stationary state M was calculated as follows:

$$G_{aq}(M) = E_p(M) + \Delta G^{corr}(M) \quad (1)$$

where $E_p(M)$ is the potential energy calculated at the PCM-ONIOM(mPW1PW91/6-311 + $G(d, p)$//PM6) level of theory on the (in vacuo) optimized structure and $\Delta G^{corr}(M)$ represents the thermal and entropic corrections to Gibbs free energy at $T = 298$ K and $p = 1$ atm obtained by in

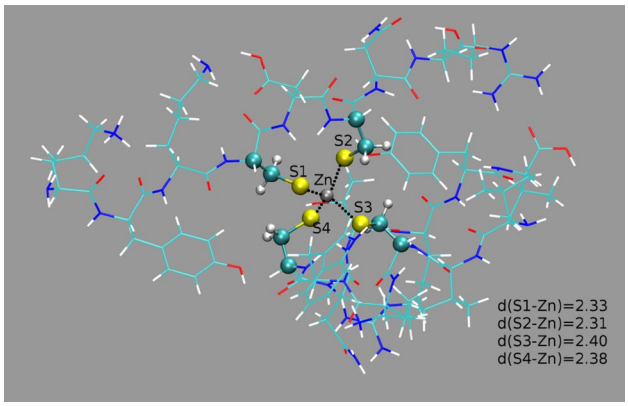

Fig. 1 Optimized protein fragment representing the zinc center of Hsp in its native state (NAT). The atoms treated at the high level of theory are represented by *spheres* and the protein environment by *lines*. The interatomic distances are given in Å

vacuo frequency calculations. The reaction energy barriers were calculated as the difference between the Gibbs free energy of the transition state and that of the free reactants (FR).

The starting configuration in the optimization of a transition state for cysteine oxidation was constructed according to the TS geometry already reported for the oxidation of the free zinc–thiolate tetrahedral complexes [14]. In the case of the S–S bridges formation, the related starting configuration for the TS optimization was obtained by exploring the potential energy surface with respect to the S–S distance. Practically, this was done by performing constrained optimizations as a function of this distance. The starting configuration for the TS optimization is the point of maximum energy identified along this curve. The nature of all transition states was checked by performing frequency calculations: in all cases, only one imaginary frequency was present.

Results and discussion

Oxidative reactivity of the four cysteine residues of the Hsp33 zinc center

The cysteine oxidation by H_2O_2 is described by the equation [4]:

$$CysS^- + H_2O_2 + H^+ \rightarrow CysSOH + H_2O \quad (2)$$

where $CysS^-$ is the deprotonated cysteine. The reaction mechanism consists in the addition of an oxygen atom of H_2O_2 to the sulfur followed by a hydrogen atom transfer to the second oxygen atom of the oxidizing agent [27]. The reaction products are the sulfonate $CysSO^-$ (that, at neutral pH, is quickly protonated) and a molecule of water.

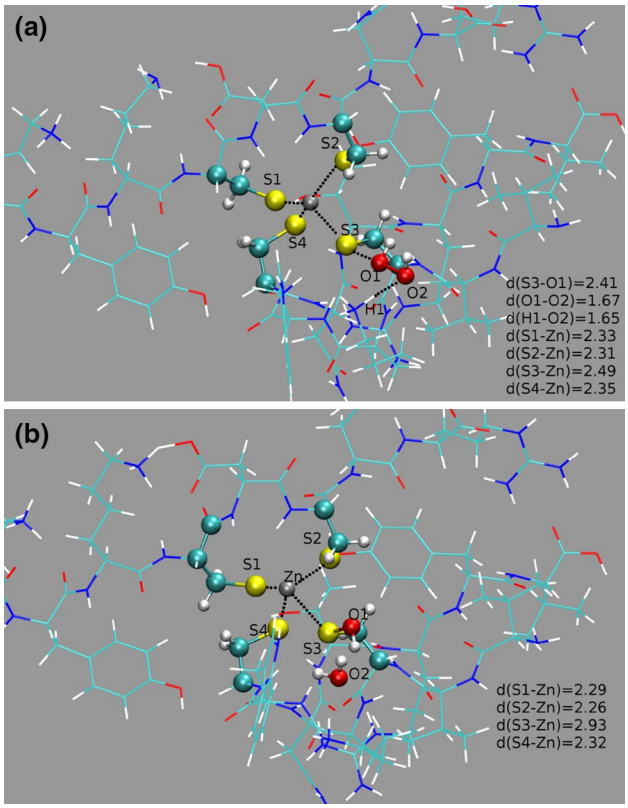

Fig. 2 Oxidation of cysteine residue Cys263: **a** the transition state (TSc) and **b** the reaction product OX1. The interatomic distances are given in Å

Obviously, the starting point for the oxidation of the zinc center of Hsp33 is dependent on the relative reactivities of the four cysteine residues present. The protein fragment representing the zinc center in its native state (NAT) was first optimized by freezing the N atoms belonging to the protein backbone, as indicated in the previous section. Here after, S1, S2, S3 and S4 denote the sulfur atoms carried by Cys231, Cys233, Cys263 and Cys266, respectively. It is interesting to note that the four Zn–S distances in the optimized structure (Fig. 1) are not identical; they are significantly longer for S3 and S4. This distortion with respect to the free zinc–thiolate complex is attributable to the protein environment and is expected to have consequences on the reactivity of the four ligands.

The optimized transition states for the oxidation of Cys231, Cys233, Cys263 and Cys266 were denoted TSa, TSb, TSc and TSd, respectively. Their typical structure is illustrated in Fig. 2a for the case of TSc and a comparison of their geometries is given in Table 1. Here, the active S atom is indicated by a star and O1 is the oxygen atom of H_2O_2 involved in the addition to the sulfur (the other oxygen atom of H_2O_2 is O2). According to the data in Table 1, the most significant differences are observed for the S*–O1

Table 1 Main geometrical parameters (in Å) of the transition states involved in the oxidation by H_2O_2 of the four cysteine residues in the zinc center of Hsp33

TS	O1–S*[a]	O1–O2	S231–Zn	S233–Zn	S263–Zn	S266–Zn	H-bonds
TSa	2.11	1.91	2.41*	2.30	2.36	2.35	–
TSb	2.20	1.83	2.30	2.41*	2.38	2.36	O2–ASN234
TSc	2.41	1.67	2.33	2.31	2.49*	2.35	O2–LYS264
TSd	2.17	1.83	2.31	2.30	2.37	2.44*	O2–THR268

[a] The star indicates the active S atom

Table 2 Gibbs free energy barriers ($\Delta G^{\ddagger}$) for the oxidation by H_2O_2 of the four cysteine residues in the zinc center of Hsp33

Transition state	Oxidized cysteine	$\Delta G^{\ddagger}$ (kcal mol^{-1})
TSa	Cys231	28.0
TSb	Cys233	24.2
TSc	Cys263	15.4
TSd	Cys266	20.3

and O1–O2 distances. One can naturally suppose that a longer S*–O1 distance (that is the distance between reactants) in the transition state is associated with a higher reactivity. From this point of view, the cysteine residue Cys263 seems to be the most reactive and Cys231 the less reactive one. All transition states excepting that for the oxidation of Cys233 are stabilized by a hydrogen bond formed between O2 and a neighboring protein residue (Table 1, last column).

A direct quantification of the reactivity of the four cysteines is obtained by calculating the (Gibbs free) energy barriers involved in their oxidation. The values given in Table 2 vary between 15 and 28 kcal mol^{-1}. Interestingly, the most reactive cysteines (Cys263 and Cys266) are those bound to zinc by longer S–Zn bonds (Fig. 1), while the less reactive (Cys231) is that for which there is no stabilizing H-bond in the transition state (Table 1). The data in Tables 1 and 2 partially confirm the correlation between the S*–O1 distance and the reaction energy barrier (the exception is observed when comparing Cys233 and Cys266, which have very similar S*–O1 distances but different reaction energy barriers).

The lowest energy barrier in Table 2 is only 1.0 kcal mol^{-1} lower than that calculated for a free zinc–thiolate complex using an equivalent computational method [14]. The other values in Table 2 suggest that more often the protein environment has a rising effect on the energy barrier of this reaction. This tendency is also confirmed by the energy barriers calculated for the zinc–cysteine cluster in the β-domain of metallothionein [22].

The most interesting prediction of the present analysis is that among the four cysteine residues in the zinc center of Hsp33 there is one (Cys263) that is significantly more reactive than the others. This implies that the first step in the global oxidation process is usually the oxidation of Cys263.

Since the pK_a and the H_2O_2 reactivity of a Zn-complexed cysteine are both dependent on the cysteine nucleophilicity, it is interesting to test if there is any correlation between the two parameters in the case of the Hsp33 active center. The calculated pK_a values of the Zn-complexed Cys231, Cys233, Cys263 and Cys266 were 2.3, 7.1, 0.0 and 1.8, respectively. The absolute pK_a values reported here should be considered with caution since our computation method was neither optimized nor tested for accurate pK_a calculations. However, in the present analysis only the relative pK_a values (that are more reliable) are relevant. If the cysteine nucleophilicity were the only important factor governing the two kinds of process, one would expect the higher p*K*a values to be associated with the higher H_2O_2 reactivities; actually, it is not the case. This result strongly suggests that the environment interactions (such as hydrogen bonding) play an important role at least in one of the two kinds of process. For instance, the high p*K*a value of Cys233 could be attributed to a hydrogen bond formed between the protonated cysteine and the side chain of Tyr270 residue. However, giving the system complexity, these preliminary results about the correlation between the p*K*a value and cysteine reactivity need further investigation.

Formation of the S–S bridges and the zinc release

Oxidation of the first cysteine residue induces some structural distortions of the zinc complex, as indicated by the oxidation product (OX1) in Fig. 2b: S3 is displaced at 2.93 Å with respect to Zn and the three other S atoms form a quasi-trigonal (hence plan) complex centered on the metal. The oxidized sulfur (S3) could in principle react with another S atom to form a first S–S bridge according to the reaction:

$$\mathrm{CysSOH} + \mathrm{CysS^-} + \mathrm{H^+} \rightarrow \mathrm{CysS-SCys} + \mathrm{H_2O} \quad (3)$$

Reaction 3 is a nucleophilic substitution and is practically diffusion limited in the case of free reactants in

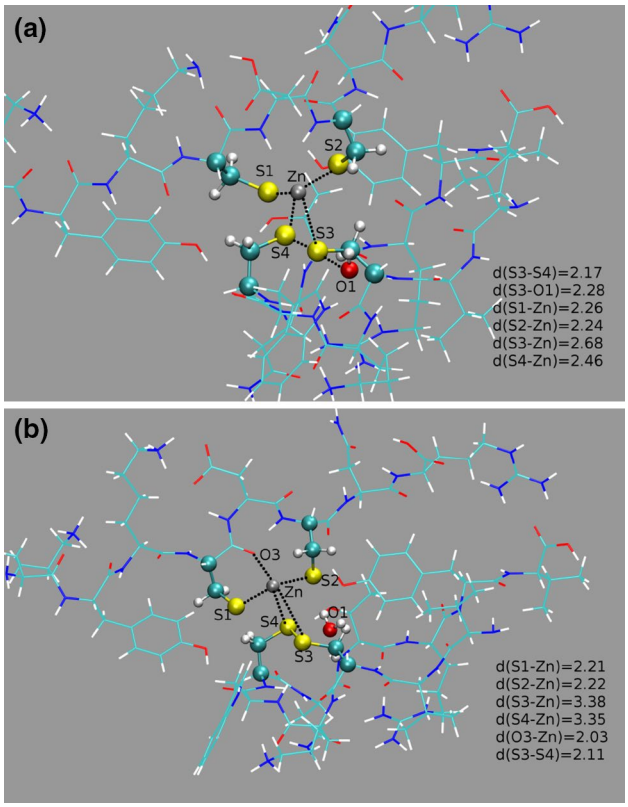

Fig. 3 Formation of the first S–S bridge (Cys263–Cys266): **a** the transition state (TS2) and **b** the reaction product OX1_SS. The interatomic distances are given in Å

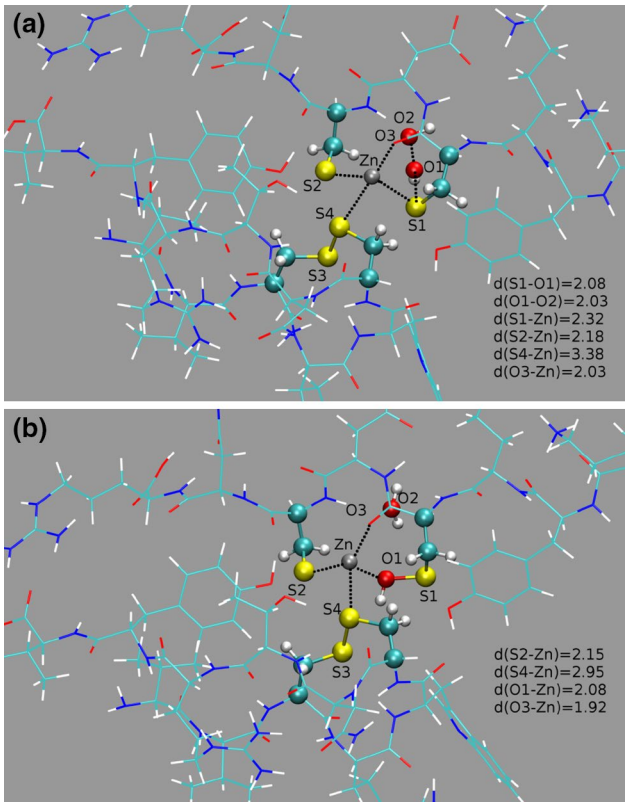

Fig. 4 The third reaction step, oxidation of Cys231 by H_2O_2: **a** the transition state (TS3) and **b** the reaction product OX2_SS. O3 is the oxygen atom of the carbonyl group of Cys231. The interatomic distances are given in Å

aqueous solution [14]. One notes also that, besides the S–S bridge, the other primary product of this nucleophilic substitution is the HO^- which at neutral pH is quickly protonated to give H_2O. At a first sight, since the distances of S3 to the three other sulfur atoms are very similar, any one of these atoms could participate with almost equal probabilities in reaction 3. However, the mechanism of the nucleophilic substitution requires the participant atoms (the two S atoms and the O atom) to be quasi-collinear. An analysis of the OX1 structure gives the following values for the corresponding S–S–O angles: S4–S3–O1 = 168°, S1–S3–O1 = 108° and S2–S3–O1 = 105°. Hence, the conformation the most favorable for the S–S bridge formation is that relaying S4, S3 and O1. For S1 and S2, the reaction is possible only after additional conformation changes. The transition state for the formation of the bridge S3–S4 (TS2) is presented in Fig. 3a. It is associated to a calculated Gibbs free energy barrier of 13.6 kcal mol^{-1}. This moderate energy barrier together with the close proximity of the two reactants indicates that the formation of the first S–S bridge occurs very quickly after the oxidation of the first cysteine. Moreover, the high rate of the reaction between the oxidized Cys263 and the reduced Cys266 can explain why an S–S bridge formed between Cys263 and Cys231 or Cys233 has never been experimentally observed.

The formation of this first S–S bridge strongly affects the structure of the zinc center, as shown by the reaction product (OX1_SS) in Fig. 3b. The S3–Zn and S4–Zn distances increase to 3.38 and 3.35 Å, respectively, while S1 and S2 are now located at 2.21 and 2.22 Å, respectively, from the metal atom. The last two values are close to those characteristic of a dicoordinated zinc–thiolate complex. A new ligand, the carbonyl group of Cys231, comes now in close contact with the zinc atom, as indicated by the distance O3–Zn that is only 2.03 Å.

The advance of the global oxidation reaction implies the oxidation of a new cysteine residue. The data in Table 2 would suggest that the next oxidation target is Cys233, which appears as more reactive than Cys231. However, this reactivity order could have been modified by the important distortion of the zinc center induced by the first two reaction steps. Consequently, we recalculated the Gibbs free energy barriers for the oxidation of Cys231 and Cys233 corresponding to the new structure (OX1_SS) of the zinc complex. The new values are 20.4 kcal mol^{-1} for the oxidation of Cys231 and 22.5 kcal mol^{-1} for the oxidation of Cys233.

They are significantly lower than those calculated for the native structure. This means that the first two reaction steps, the first cysteine oxidation and the first S-S bridge formation, respectively, open the way for the oxidation of the two less reactive cysteines. In the new molecular conformation, Cys231 becomes more reactive than Cys233 and, in our calculations, it was considered as the next target of H_2O_2. The corresponding transition state (TS3) and oxidation product (OX2_SS) are given in Fig. 4a, b, respectively.

The fourth step in the overall oxidation process starts from the oxidation product OX2_SS. It could consist in the formation of the bridge S1–S2. However, the actual conformation of the zinc center is not very favorable to this reaction. Indeed, the oxygen atom of the sulfenic acid formed in the preceding reaction step participates in the zinc complex as a ligand (Fig. 4b). A significant reorganization of the complex is thus necessary to bring S1, S2 and O1 in a position allowing the formation of the second S–S bridge. We forced this reorganization by performing constrained optimizations as a function of the S1–S2 distance. The potential energy profile thus obtained led, after a subsequent unconstrained optimization, to the transition state TS4 (Fig. 5a) and to the product OX2_2SS (Fig. 5b). As expected, the corresponding Gibbs free energy barrier for the formation of this second S–S bridge is high, 34.8 kcal mol^{-1}. We have already mentioned that the formation of S–S bridges from free reactants is near diffusion limited. Hence, the main contribution to this high energy barrier can be attributed to the structural constrains imposed by the protein environment. Finally, the formation of a second S–S bridge in the present molecular conformation can be considered as very unlikely.

An alternative reaction step may consist in a direct oxidation of Cys233 by H_2O_2. The starting structure to be considered for this reaction is the intermediate product OX2_SS. The Gibbs free energy barrier thus calculated is 21.4 kcal mol^{-1}. This value predicts that the direct oxidation of Cys233 in the present molecular conformation is a possible process, although it appears to be slower than the three preceding reaction steps.

It is very interesting to compare these predictions to the experimental results of the in vitro oxidation of Hsp33 zinc center by H_2O_2 reported by Ilbert et al. [8]. When the reaction was conducted at 30 °C, the authors detected an intermediate product for which only one of the cysteine residues Cys231 and Cys233 was in the oxidized form, while the zinc was already released from the protein structure. Instead, for a reaction temperature of 43 °C, all the cysteine residues were in their oxidized form. To account for these results, the authors proposed a mechanism in which, after the formation of the first S–S bridge and the direct oxidation of the third cysteine, the zinc is completely released. The formation of the second S–S bridge becomes kinetically allowed only after a partial protein unfolding following the zinc release. This partial unfolding is much more probable at 43 °C than at 30 °C thus explaining the persistence of the partially oxidized intermediate at this later temperature. To test this hypothesis, we investigated the probability of a zinc release starting from the OX2_SS state. The structure of the model protein fragment

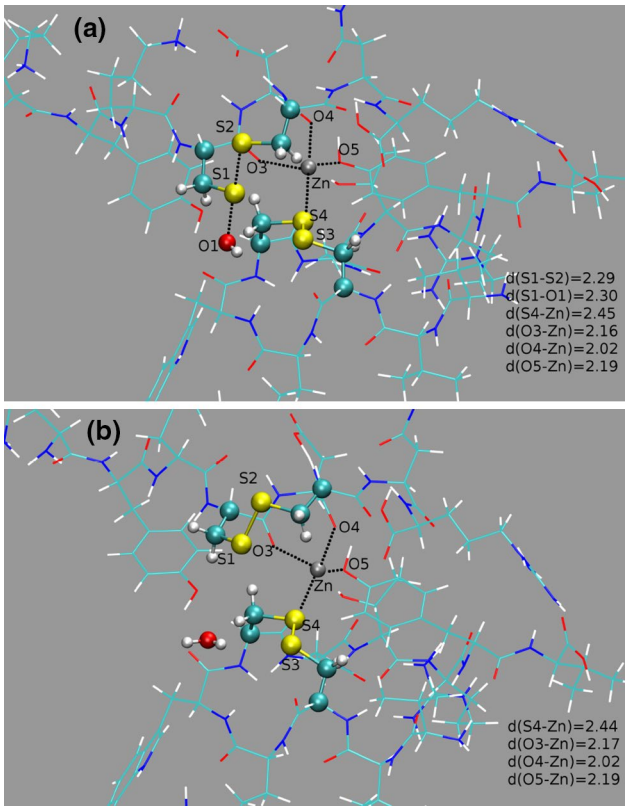

Fig. 5 Formation of the second S–S bridge prior the release of zinc: **a** the transition state (TS4) and **b** the reaction product OX2_2SS. O3 belongs to Cys231, O4 to Asp232 and O5 to Lys270. The interatomic distances are given in Å

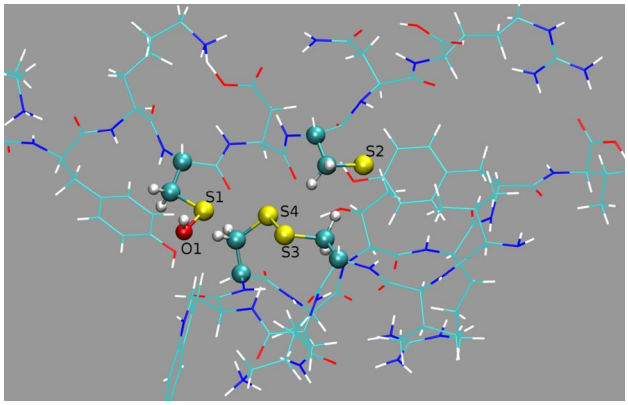

Fig. 6 Optimized protein fragment representing the zinc center of Hsp33 after the release of zinc (APO1)

optimized after removing the zinc cation (APO1) is given in Fig. 6.

It is very likely that this structure describes only an intermediate state related to the local minimum on the potential energy surface that is nearest with respect to the starting conformation OX2_SS. In reason of the very important structural role of the zinc cation, it is expected that its release induces further conformational changes that will stabilize the apoprotein. Obviously, the present computational method is not appropriate for modeling this subsequent protein unfolding. It is, however, possible to calculate the change in the Gibbs free energy (ΔG_d) upon the transition between the OX2_SS and APO1 states:

$$\Delta G_d = G(\text{APO1}) + G(\text{Zn}^{2+}_{aq}) - G(\text{OX2\_SS}) \quad (4)$$

In evaluating the Gibbs free energy of Zn^{2+} in aqueous solution, we used the experimental value for the solvation energy of this cation which is 479.1 kcal mol^{-1}. This value was obtained by correcting the solvation energy given in Ref. [28] that was originally compiled using a proton solvation energy of −252.6 kcal mol^{-1}. A more reliable value for this reference solvation energy is −264.0 kcal mol^{-1} [29]. The zinc dissociation Gibbs free energy calculated according to Eq. 4 was 6.0 kcal mol^{-1}. Based on this value, one can evaluate the relative abundance of the OX2_SS and APO1 species in cytosol. The corresponding equilibrium constant K is expressed as:

$$K = \frac{1}{c_0}\frac{[\text{APO1}]_{eq}\left[\text{Zn}^{2+}\right]_{eq}}{[\text{OX2\_SS}]_{eq}} = \exp(-\Delta G_d/RT) \quad (5)$$

where c_0 is the standard molar concentration in aqueous solution (1 mol L^{-1}), R the universal constant of gas and T the absolute temperature. Given the fact that the cytosolic concentration of free Zn^{2+} is smaller than 10^{-9} mol L^{-1} [30], one finds that at equilibrium, the ratio between the concentrations of the APO1 and OX2_SS forms is greater than $10^{4.7}$. When the subsequent protein unfolding is taken into account, the concentration of the OX2_SS form will be still smaller. The formation of APO1 is also kinetically favored. Indeed, the complexation rate constant k_c and the dissociation rate constant k_d are relied by the following relation:

$$\frac{k_d}{k_c} = c_0 K = c_0 \exp(-\Delta G_d/RT) \quad (6)$$

Normally, the complexation reaction has no energy barrier since it does not involve any bond breaking. Hence, one can assume that the zinc–protein complexation is diffusion limited (that is $k_c \approx 10^{10}$ s^{-1} mol^{-1} L). Under this hypothesis, Eq. 6 gives a value of the order of 10^6 s^{-1} for k_d. This means that OX2_SS is rather a short-lived state. Thus, the reaction steps alternative to the zinc release (that is the direct oxidation of Cys233 or the formation of the second S–S bridge) are unlikely given their high energy barriers. In conclusion, the present theoretical results are clearly compatible with the reaction mechanism proposed in Ref. [8].

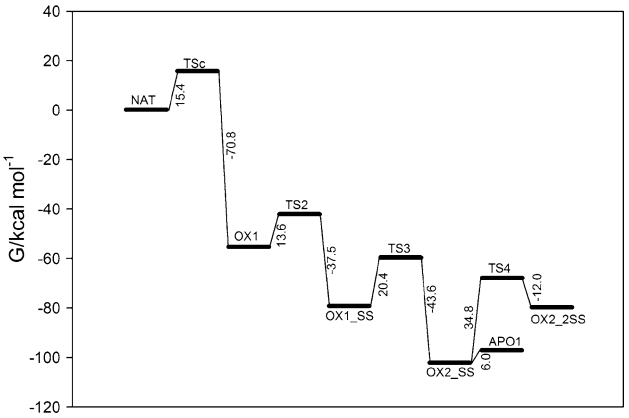

Fig. 7 Gibbs free energy diagram of transition states and intermediary products involved in the mechanism of oxidation by H_2O_2 of Hsp33 zinc center. Here, NAT denotes the free reactants, TSc the transition state for oxidation of Cys263 by H_2O_2, OX1 the product of this reaction, TS2 the transition state for the formation of the first S–S bridge (Cys263–Cys266), OX1_SS the product of this reaction, TS3 the transition state for the subsequent oxidation of Cys231 by H_2O_2, OX2_SS the product of this reaction, TS4 the transition state for the formation of the second S–S bridge, OX2_2SS the product of this reaction, APO1 the product of the Zn release (before formation of the second S–S bridge)

A synthetic description of the complete step-by-step reaction sequence predicted by our analysis is depicted in Fig. 7. The Gibbs free energy levels in this diagram give information about the stability of the reaction intermediates as well as about the reaction rates involved in the different transitions. The slower step in this sequence appears to be the oxidation of the second cysteine residue by H_2O_2 (TS3). In the transition state theory, the reaction rate constant (k) and the reaction Gibbs free energy barrier ($\Delta G^{\ddagger}$) are related by [27]:

$$k = (K_B T/h)\exp(-\Delta G^{\ddagger}/RT) \quad (7)$$

where K_B is the Boltzmann constant and h the Planck constant. Using the Gibbs free energy barriers calculated for TS1 and TS3 one obtains for the first and the second cysteine–H_2O_2 reaction a rate constant of 0.4 × 10^2 and 1.0 × 10^{-2} s^{-1} mol L^{-1}, respectively (calculated for T = 298 K). Detailed kinetics data about the oxidation of the zinc center of Hsp33 have not been reported yet. In the in vitro experiments of Ilbert et al. [8] performed at t = 30 °C for a H_2O_2 concentration of 4 × 10^{-3} mol L^{-1}, the oxidation process was completed after about 180 min. The theoretical rate constants derived here give for the same H_2O_2 concentration a reaction halftime of 4 s for the first

cysteine–H_2O_2 reaction and of 288 min for the second. Given the fact that the second oxidation is the limiting step of the global reaction, one concludes that our theoretical reaction energy barriers are in satisfactory agreement with the experimental data reported so far. When making this comparison one should keep in mind the fact that a variation in the energy barrier of only 2 kcal mol^{-1} is equivalent to the change of the reaction halftime by a factor of about 25.

Concluding remarks

In this work, we use the methods of quantum chemistry to give a detailed picture of the global oxidation of Hsp33 zinc center. According to these predictions, the oxidation always starts at the same point: the cysteine residue Cys263. It is likely that this constancy participates to the control exerted by the protein environment on the reaction pathway. Another efficient control point of the reaction pathway is the formation of S–S bridges. Indeed, since this reaction has no energy barrier when occurring between free reactants, its rate can be efficiently regulated by the conformation of the zinc center. The reproducibility of the reaction intermediates and of their conformations appears to be the main reason of the absence of wrong S–S bridges formed between cysteine residues that are distant in the primary protein structure.

The reliability of the theoretical results here reported is reinforced by their agreement with the experimental data on the oxidation of Hsp33 available to date. However, additional theoretical and experimental work is still necessary to clarify the next step in the Hsp33 activation that is the protein unfolding following the zinc release.

Acknowledgments Calculations were carried out largely with the supercomputer facility at the Mésocentre, a regional computational center at the University of Franche-Comté.

References

1. Groitl B, Jakob U (2014) Biochim Biophys Acta 1844:1335–1343
2. Klomsiri CP, Karplus PA, Poole LB (2011) Antiox Redox Sign 14:1065–1077
3. Brandes N, Schmitt S, Jakob U (2009) Antiox Redox Sign 11:997–1014
4. Winterbourn CC, Metodiewa D (1999) Free Rad Biol Med 27:322–328
5. Kortemme T, Creighton TE (1995) J Mol Biol 253:799–812
6. Wedemeyer WJ, Welker E, Narayan M, Scheraga HA (2000) Biochem. 39:4207–4216
7. Winter J, Ilbert M, Graf PCF, Özcelik D, Jakob U (2008) Cell 135:691–701
8. Ilbert M, Horst J, Ahrens S, Winter J, Graf PCF, Lilie H, Jakob U (2007) Nat Struct Mol Biol 14:556–563
9. Graf PCF, Martinez-Yamout M, VanHaerents S, Lilie H, Dyson HJ, Jakob U (2004) J Biol Chem 279:20529–20538
10. Jaroszewski L, Schwarzenbacher R, McMullan D, Abdubek P, Agarwalla S, Ambing S, Axelrod H, Biorac T, Canaves JM, Chiu H-J, Deacon AM, DiDonato M, Elsliger M-A, Godzik A, Grittini C, Grzechnik SK, Hale J, Hampton E, Han GW, Haugen J, Hornsby ME, Klock HE, Koesema E, Kreusch A, Kuhn P, Lesley SA, Miller MD, Moy K, Nigoghossian E, Paulsen J, Quijano K, Reyes R, Rife C, Spraggon G, Stevens RC, van den Bedem H, Velasquez J, Vincent J, White A, Wolf G, Xu Q, Hodgson KO, Wooley J, Wilson IA (2005) Prot Struct Func Bioinf 61:669–673
11. Graumann J, Lilie H, Tang X, Tucker KA, Hoffmann JH, Vijayalakshmi J, Saper M, Bardwell JCA, Jakob U (2001) Struct 9:377–387
12. Barbirz S, Jakob U, Glocker MO (2000) J Biol Chem 275:18759–18766
13. Reichmann D, Jakob U (2013) Curr Opin Struct Biol 23:436–442
14. Kassim R, Ramseyer C, Enescu M (2011) Inorg Chem 50:5407–5416
15. Adamo C, Barone V (1998) J Comp Chem 19:418–429
16. Warshel A, Levitt M (1976) J Mol Biol 103:227–249
17. Lin H, Truhlar DG (2007) Theor Chem Acc 117:185–199
18. Yao L, Cukier RI, Yan H (2007) J Phys Chem B 111:4200–4210
19. Wang J, Sklenak S, Liu A, Felczak K, Wu Y, Li Y, Yan H (2012) Biochem 51:475–486
20. Yang W, Drueckhammer DG (2003) J Phys Chem B 107:5986–5994
21. Stewart JJP (2007) J Mol Model 13:1173–1213
22. Kassim R, Ramseyer C, Enescu M (2013) J Biol Inorg Chem 18:333–342
23. Frisch MJ, Trucks GW, Schlegel HB, Scuseria GE, Robb MA, Cheeseman JR, Scalmani G, Barone V, Mennucci B, Petersson GA, Nakatsuji H, Caricato M, Li X, Hratchian HP, Izmaylov AF, Bloino J, Zheng G, Sonnenberg JL, Hada M, Ehara M, Toyota K, Fukuda R, Hasegawa J, Ishida M, Nakajima T, Honda Y, Kitao O, Nakai H, Vreven T, Montgomery Jr. JA, Peralta JE, Ogliaro F, Bearpark M, Heyd JJ, Brothers E, Kudin KN, Staroverov VN, Kobayashi R, Normand J, Raghavachari K, Rendell A, Burant JC, Iyengar SS, Tomasi J, Cossi M, Rega N, Millam NJ, Klene M, Knox JE, Cross JB, Bakken V, Adamo C, Jaramillo J, Gomperts R, Stratmann RE, Yazyev O, Austin AJ, Cammi R, Pomelli C, Ochterski JW, Martin RL, Morokuma K, Zakrzewski VG, Voth GA, Salvador P, Dannenberg JJ, Dapprich S, Daniels AD, Farkas Ö, Foresman JB, Ortiz JV, Cioslowski J, Fox DJ (2009) Gaussian 09, Revision A.02, Gaussian Inc., Wallingford CT
24. Svensson M, Humbel S, Morokuma K (1996) J Chem Phys 105:3654–3661
25. Dapprich S, Komáromi I, Byun KS, Morokuma K, Frisch MJ (1999) J Mol Struct (Theochem) 462:1–21
26. Cossi M, Scalmani G, Rega N, Barone V (2002) J Chem Phys 117:43–54
27. Cardey B, Enescu M (2005) Chem Phys Chem 6:1175–1180
28. Marcus Y (1991) J Chem Soc Faraday Trans 87:2995–2999
29. Kelly CP, Cramer CJ, Truhlar DG (2006) J Phys Chem B 110:16066–16081
30. Colvin RA, Holmes WR, Fontainea CP, Maret W (2009) Metallomics 2:297–356